Since January 2020 Elsevier has created a COVID-19 resource centre with free information in English and Mandarin on the novel coronavirus COVID-19. The COVID-19 resource centre is hosted on Elsevier Connect, the company's public news and information website.

Elsevier hereby grants permission to make all its COVID-19-related research that is available on the COVID-19 resource centre - including this research content - immediately available in PubMed Central and other publicly funded repositories, such as the WHO COVID database with rights for unrestricted research re-use and analyses in any form or by any means with acknowledgement of the original source. These permissions are granted for free by Elsevier for as long as the COVID-19 resource centre remains active.

Computers in Biology and Medicine 145 (2022) 105452

Contents lists available at ScienceDirect

Computers in Biology and Medicine

journal homepage: www.elsevier.com/locate/compbiomed

Multidimensional in silico strategy for identification of natural polyphenols-based SARS-CoV-2 main protease (M^{pro}) inhibitors to unveil a hope against COVID-19

Şevki Adem [a], Volkan Eyupoglu [a,*], Ibrahim M. Ibrahim [b], Iqra Sarfraz [c], Azhar Rasul [c,**], Muhammad Ali [d], Abdo A. Elfiky [b,***]

[a] Department of Chemistry, Faculty of Science, Cankiri Karatekin University, 18100, Cankırı, Turkey
[b] Biophysics Department, Faculty of Science, Cairo University, Giza, Egypt
[c] Cell and Molecular Biology Lab, Department of Zoology, Faculty of Life Sciences, Government College University Faisalabad, 38000, Faisalabad, Pakistan
[d] Vice Chancellor, Quaid-i-Azam University, Islamabad, Pakistan

ARTICLE INFO

Keywords:
COVID-19
SARS CoV-2 M^{pro}
Molecular docking
Molecular dynamics simulation
Quantum mechanic
Flavonoids

ABSTRACT

SARS-CoV-2, a rapidly spreading new strain of human coronavirus, has affected almost all the countries around the world. The lack of specific drugs against SARS-CoV-2 is a significant hurdle towards the successful treatment of COVID-19. Thus, there is an urgent need to boost up research for the development of effective therapeutics against COVID-19. In the current study, we investigated the efficacy of 81 medicinal plant-based bioactive compounds against SARS-CoV-2 M^{pro} by using various in silico techniques. The interaction affinities of polyphenolic compounds towards SARS-CoV-2 M^{pro} was assessed via intramolecular (by Quantum Mechanic), intermolecular (by Molecular Docking), and spatial (by Molecular Dynamic) simulations. Our obtained result demonstrate that Hesperidin, rutin, diosmin, and apiin are most effective compounds agents against SARS-CoV-2 Mpro as compared to Nelfinavir (positive control). This study will hopefully pave a way for advanced experimental research to evaluate the *in vitro* and *in vivo* efficacy of these compounds for the treatment of COVID-19.

1. Introduction

An acute respiratory disorder caused by 2019-novel coronavirus [2019-nCoV, now known as SARS-CoV-2 (severe acute respiratory syndrome coronavirus-2)] has emerged as a serious public health issue at the end of 2019 [1]. During the 21st century, COVID-19 marked the history with the third large-scale coronavirus epidemic into the human population after SARS-CoV in 2002 in china [2] and Middle East respiratory syndrome coronavirus (MERS-CoV) in the Middle East region in 2012 [3]. The potentially fatal virus has affected millions of humans around the world and this pandemic is still steadily spreading [4]. Researchers have developed vaccines for COVID-19, however, research suggests that developed vaccines will not completely enough to fight against COVID-19 due to high mutation rate of SARS CoV2 [5]. The recommended HIV protease inhibitors (Nelfinavir, Lopinavir, and Ritonavir), antibody cocktail, and other virus-fighting drugs have very limited potential to cure COVID-19 [5,6]. Thus, there is an urgent need to develop therapeutics for COVID-19.

The structure of SARS CoV-2 has been identified as β-coronavirus, a non-segmented enveloped positive-sense RNA virus, with ~30 kb genome [7,8]. SARS CoV-2 causes severe respiratory tract infection and utilizes angiotensin-converting enzyme 2 (ACE2) receptors to infect human cells [9]. The crystallized form of SARS CoV-2 virus main protease (M^{pro}) was demonstrated by a Chinese researcher Liu et al. [10], which is a potential drug target for the inhibition of SARS CoV-2 replication [11]. The M^{pro} is an essential protein required for the proteolytic cleavage of viral polypeptide [12] to release functional proteins such as endoribonuclease, exoribonuclease, and RNA polymerase [13]. The functional significance of M^{pro} in the SARS CoV-2 life cycle [15], as well as the absence of its close homologs in humans, identify M^{pro} as an

* Corresponding author.
** Corresponding author.
*** Corresponding author.
E-mail addresses: volkan@karatekin.edu.tr, chemist49@gmail.com (V. Eyupoglu), drazharrasul@gmail.com, azharrasul@gcuf.edu.pk (A. Rasul), abdo@sci.cu.edu.eg (A.A. Elfiky).

https://doi.org/10.1016/j.compbiomed.2022.105452
Received 6 May 2021; Received in revised form 13 July 2021; Accepted 23 March 2022
Available online 26 March 2022
0010-4825/© 2022 Elsevier Ltd. All rights reserved.

attractive target for antiviral drug discovery [14].

The growing evidence has established the worth of polyphenols as cheaper and safer drug candidates for drug discovery against various human diseases [16,17]. *In silico* based screening has proven to be an excellent tool to meet the challenges of drug discovery [18,19]. Additionally, Molecular Dynamics Simulation (MDS) is extremely useful in drug design against different viruses, where protein dynamics are assessed in the nano to picosecond time interval [20–26]. Molecular dynamic theory is based on the spatial conformation of molecular interactions from their active sides by intermolecular interactions like weak van der Waals interactions, London forces or hydrogen bonding, etc [27,28]. So, MD simulations are performed to obtain information about docked agents to the real (*in vitro*) experimental results. Many computational approaches have been developed to predict the absorption, distribution, metabolism, and excretion (ADME) properties of drug candidates from their physicochemical properties by comparing them with compounds. These methods, which reduce costs and save time, have now become an integral part of drug research and development studies [29].

In the current study, we have investigated the potential of 81 polyphenolic compounds against SARS CoV-2 Mpro by molecular docking via frontier molecular orbital theory by Material Studio 7.0 (MS), ADMET, and molecular dynamics by NAMD assessments. All small molecules used for docking studies were obtained from https://pubchem.ncbi.nlm.nih.gov/as SDF form and in the 3D Conformer. QM assessment of molecules was performed to elaborate the molecular docking studies. The best-fitted geometry of the molecules, highest occupied molecular orbital (HOMO), lowest unoccupied molecular orbital (LUMO), and other intermolecular parameters were calculated by MS using density functional theory (DFT). The investigated molecules were evaluated for their metabolic activities and pharmacokinetic parameter in the cell membrane, blood-brain barrier, etc. by ADMET online platform. Our obtained results indicate that hesperidin, diosmin, rutin, and apiin are best four potent inhibitors against SARS CoV-2 M^{pro}. These compounds were further tested against the SARS CoV-2 M^{pro} at different dynamics states by NAMD using CHARMM 36 forcefield in 100 ns MDS run to prove their biological activities in computer simulation conditions.

2. Materials and methods

2.1. Molecular docking studies

2.1.1. Target protein model preparation

The docking of the compounds inside SARS-CoV-2 M^{pro} was performed using Molegro Virtual Docker (MVD) and AutoDock Vina software [30,31]. The crystal structure of SARS-CoV-2 M^{pro} was retrieved from the protein data bank website (http://www.rcsb.org/pdb) (PDB ID: 6LU7 and 6Y84: Resolution 2.16 Å and 1.39 Å, respectively) [32,33]. Proteins were imported to Molegro Virtual Docker and prepared for docking. Water molecules at crystal structure were removed, protein structure errors were checked. The structure errors of amino acid residues were checked, repaired, optimized with the neighborhood residues.

2.1.2. Small molecules preparation

Small molecules or ligands used in docking studies were obtained from https://pubchem.ncbi.nlm.nih.gov/as SDF form and in the 3D Conformer [34]. They were prepared with Molegro Virtual Docker (MVD) for molecular docking.

2.1.3. Molecular docking

The selected cavity of SARS-CoV-2 M^{pro} was the binding site of natural inhibitor N3. The cavity is centered at (−10.85, 15.32, 68.39) with 15 Å radius. AutoDock Vina box size (20 × 20 × 20 Å) was centered at the active site residues around (−10.85, 15.32, 68.39) Å. Ten docking trials were performed in both software, and the compounds with best binding affinity were selected for further evaluation. Nelfinavir was utilized as a positive control. Nelfinavir is a viral protease inhibitor used for the treatment of the human immunodeficiency virus (HIV), which has been previously reported as a SARS CoV-2 M^{pro} inhibitor [35]. Possible docking modes between compounds and the COVID-19 virus M^{pro} were analyzed using the Discovery Studio 2020 Client and PyMOL software [36].

2.2. Molecular dynamic simulation

The best resolution of SARS-CoV-2 M^{pro} (PDB ID: 6Y84) was subjected to 100 ns MDS after the minimization and equilibration steps. Firstly, the protein is solvated using the TIP3P water model then ionized with NaCl [37]. NAMD was used for the minimization via using the CHARMM 36 force field [20,38,39]. After minimizing the whole system, temperature was slowly adjusted to 310 K to resemble the physiological temperature of the human body (37 °C). A small NPT MDS run was performed to adjust the system volume, followed by the production run at the NVT ensemble for 100 ns. VMD software was utilized in the analysis of the data [40].

2.3. Frontier molecular orbital modeling

The modeling of HOMO, LUMO orbitals of the most effective small molecules and target protein are calculated by density functional theory (DFT) on Material Studio 7.0 Code embedded in the Material Studio package (Accelrys, SanDiego, CA) [41] by using $DMol^3$ module [42–44].

2.4. ADMET assessment

The ADMET properties of selected compounds were analyzed by using the http://biosig.unimelb.edu.au/pkcsm/prediction website. The molecular structures of the natural compounds were uploaded using isomeric SMILES into webtool. Important results were retrieved from website for analysis [45].

3. Results and discussion

3.1. Molecular docking studies

Coronaviruses have a long history of infecting humans and animals and causing respiratory, digestive, liver, and central nervous system diseases [46]. A novel newly emerged virus, SARS-CoV-2, is presenting significant threats to human health nowadays. Currently, no specific clinical therapeutics are available for the treatment of SARS-CoV-2-mediated respiratory infections [47]. Thus, the need of the hour is to identify and characterize novel drug candidates to overcome the health losses caused by SARS-CoV-2. In this context, natural products have gained importance as potent antiviral agents during recent years [48,49]. Several computational studies suggest the significance of phytochemicals and nutraceuticals in drug development against SARS-CoV-2 [22,50–54]. Considering the immediate need for therapeutics against COVID-19 and services of natural products in drug discovery [55], we have screened flavonoids against a novel drug target, SARS-CoV-2 M^{pro}, for the identification of natural scaffolds for drug development against COVID-19.

The binding energies obtained after docking of the compounds into SARS-CoV-2 M^{pro} (PDB ID: 6LU7) are presented in Table 1. According to the in silico results, 24 of the compounds have a better affinity against COVID-19 virus M^{pro} than Nelfinavir (Fig. 1). Hesperidin exhibited the highest affinity to the active site of SARS-CoV-2 M^{pro} followed by rutin, diosmin, and apiin respectively (Fig. 1).

The amino acid residues that contribute to interactions between the reference ligand and hit compounds are demonstrated in Table 2. Glu 189, Glu 166, and Met165 are the main residues contributing for interactions between target proteins and ligands.

Table 1
Results of the docking of some phenolic compounds on the crystal structure of COVID-19 main protease.

Ligands		MolDock Score	HBond	Ligands		MolDock Score	HBond
PubChem CID	Name			PubChem CID	Name		
	N3 (Reference ligand)	−162.17	−8.19	5280343	Quercetin	−122.99	−13.97
64143	**Nelfinavir (Positive control)**	−147.38	−6.87	5280551	Xenognosin B	−119.14	−7.85
10621	Hesperidin	−178.59	−20.26	5280373	Biochanin a	−118.80	−9.65
5280805	Rutin	−176.27	−21.24	5280863	Kaempferol	−118.63	−14.28
5281613	Diosmin	−174.13	−27.26	3764	Isoformononetin	−117.02	−7.10
5280746	Apiin	−171.01	−10.19	31425	Vat Yellow 2	−116.61	−1.86
6441419	Diacetylcurcumin	−169.26	−9.57	5280378	Formononetin	−115.58	−7.39
101502236	3,3′-*m*-Phenylenebis[1-(2-hydroxy-4-methoxyphenyl)-2-propene-1-one]	−168.14	−7.74	439533	(±)-Taxifolin	−115.47	−12.37
101526067	Beta, Beta'-(4-Methoxy-1,3-Phenylene)Bis(2′-Hydroxy-4′,6′-Dimethoxyacrylophenone)	−164.87	−6.68	5280445	Luteolin	−114.90	−10.76
46702071	(E)-1-[2,6-dihydroxy-3-[(E)-3-(4-hydroxyphenyl)prop-2-enoyl]-4-methoxyphenyl]-3-(4-hydroxyphenyl)prop-2-en-1-one	−162.53	−13.65	5281670	Morin	−114.74	−14.28
44259442	Myricetin	−161.72	−16.62	97214	Eupatorin	−113.99	−12.52
5281544	Oleuropein	−160.69	−26.89	188323	Cirsimaritin	−113.98	−5.63
3035266	Flavone23	−159.64	−2.21	5281612	Diosmetin	−113.51	−8.07
442428	Naringin	−158.82	−8.59	445154	Resveratrol	−113.09	−5.76
442439	Neohesperidin	−158.33	−16.12	5281628	Hispidulin	−112.01	−7.60
969516	Curcumin	−157.92	−10.50	54685921	Hispidin	−110.03	−11.94
185617	Scutellarin	−157.90	−14.20	5281708	Daidzein	−109.72	−7.58
114627	Neoeriocitrin	−157.58	−18.62	5281616	Galangin	−109.69	−10.31
	Daidzein	−157.41	−7.08	5281697	Scutellarein	−108.52	−14.50
6419835	(−)-Catechin gallate	−156.13	−16.87	5280443	Apigenin	−108.11	−11.77
44259136	Quercetin 3-β-D-glucoside	−156.08	−17.24	68077	Tangeritin	−107.75	−2.09
64982	Baicalin	−153.60	−12.10	5281894	7-Hydroxyflavone	−106.62	−5.58
168849	Pectolinarin	−152.42	−9.01	932	Naringenin	−106.38	−12.13
5281718	Polydatin	−151.85	−13.86	5281607	Chrysin	−105.48	−5.74
5282151	Vitexin 2-*o*-rhamnoside	−150.02	−17.63	72276	(−)-epicatechin	−103.49	−11.21
71602340	Balsacone A	−149.70	−14.08	72281	Hesperitin	−102.36	−8.96
5469424	Scutellaric Acid	−102.01	−2.17	5281703	Wogonin	−98.56	−8.71
46781931	Quercetin 3-D-galactoside	−148.42	−11.77	637775	Sinapinic acid	−98.54	−2.49
5315472	Bisdemethoxycurcumin	−144.47	−8.52	11349	3-Hydroxyflavone	−97.65	−3.33
73447	Uvaretin	−140.06	−5.08	5281605	Baicalein	−95.74	−11.12
23640558	Curcumin Pyrazole	−139.95	−8.77	68112	5-Hydroxyflavone	−95.71	−2.45
56842347	Oleuropein aglycone	−138.79	−14.31	72279	6-Hydroxyflavone	−94.09	−3.46
151670	Isouvaretin	−133.17	−9.08	5281855	Ellagic acid	−93.64	−13.37
11652416	Oleocanthal	−132.88	−15.19	10680	Flavone	−91.48	0.00
5320945	Rhamnazin	−132.22	−11.87	445858	ferulic	−87.97	−4.89
18684078	Oleacein	−130.73	−11.41	10742	syringic acid	−86.68	−5.44
4303567	Acacetin Diacetate	−130.16	−12.80	689043	Caffeic acid	−85.71	−6.71
638278	Isoliquiritigenin	−128.09	−10.42	114850	Oxymatrine	−84.27	−0.56
31553	Silibinin	−127.04	−18.58	637542	*p*-Coumaric acid	−80.83	−4.11
65084	(+)-gallocatechin	−126.55	−17.54	8468	Vanillic	−78.61	−4.56
162464	Cirsilineol	−126.48	−11.81	54670067	L-Ascorbic acid	−77.10	−15.98
5281377	Genistin	−126.28	−12.71	8742	Shikimic acid	−76.85	−6.74
5281614	Fisetin	−123.53	−13.67	370	Gallic acid	−75.87	−10.65
124052	Glabridin	−123.00	−5.16	1491	3,4-Dihydroxybenzoic acid	−72.59	−4.00

Hesperidin exhibited the highest binding energy at the active site of SARS-CoV-2. 2D and 3D interaction diagrams are provided in Fig. 2. Hesperidin formed hydrogen bond interactions with Thr 26, Glu 166, Arg 188, Gln 189, Met 49, Asp 187, His 163, Leu 141, and Ser 144 residues. B ring of flavonoid structure formed Pi-Sulfur interacts with Cys 145. Further about 10 amino acids contributed to the stabilization of the molecule in the active site via van der Waals interactions.

The obtained results showed that His 41, Cys 145, Phe 140, Glu 166, Gln 192, Thr 190, and His 164 are critical residues for the hydrogen bonding interactions at the binding site of rutin to protease protein (Fig. 3). Hydrophobic interactions such as Pi-Pi T-shaped, Amide-Pi Stacked, and Pi-Alkyl were responsible for interactions between target protein and ligands. Cys 145 interacted with both phenyl rings and a heterocyclic ring to form pi-sulfur interaction.

The interacting amino acids for diosmin and apiin are presented in Figs. 4 and 5.

SARS main protease enzymes have a protease Cys-His dyad created by Cys145 and His41 residues. The reported protease inhibitors interact with Cys145 [56]. Diosmin, Apiin, and Rutin form a hydrogen bond with this catalytic amino acid, while Hesperidin interacts via pi-sulfur interaction. Table 1 demonstrates that these natural compounds form strong interactions with His41. 2D interaction models showed that Hesperidin and Apiin forms van der Waals interaction with His41 and Diosmin and rutin form hydrogen bond interactions.

3.2. Quantum mechanic studies

3.2.1. General chemical reactivities by HOMO-LUMO estimation

Global Reactivity Descriptors based on the HOMO and LUMO energy differences are very important indicators to determine the reactive affinity of molecules against nucleophilic electrophilic and radicalic attacks. All descriptors or indexes were calculated by well-known equations (Eqs. (1)–(5)) according to the literature [57,58].

$$\eta = 1/2\ (E_{LUMO} - E_{HOMO}) \quad \text{(Eq.1)}$$

$$S = 1/2\ \eta \quad \text{(Eq.2)}$$

$$\omega = \mu^2/2 \quad \text{(Eq.3)}$$

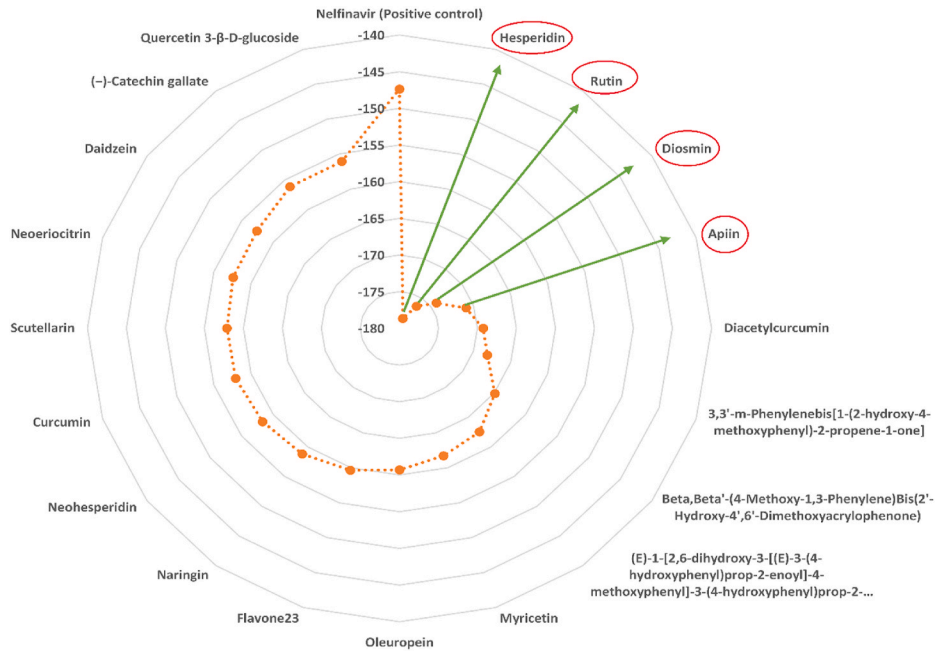

Fig. 1. MolDock docking experiment (A) MolDock scores calculated for the best 24 natural polyphenols and Nilfinavir against the SARS-CoV-2 M^{pro}. (B) Summary of the in silico based screening of natural product library and identification of potential natural inhibitors of SARS-CoV-2 M^{pro}.

Table 2
The ten amino acid residues at the active cavity interacting with the reference inhibitor and ligands.

Hesperidin			Rutin			Diosmin			Apiin			N3		
Residue	**ID**	**Total**	**Residue**	**ID**	**Total**	**Residue**	**ID**	**Total**	**Residue**	**ID**	**Total**	**Residue**	**ID**	**Total**
Glu	**166**	**−37.06**	**Gln**	**189**	**−31.49**	**Glu**	**166**	**−28.64**	**Gln**	**189**	**−24.03**	**Glu**	**166**	**−28.623**
Gln	**189**	**−20.72**	**Met**	**165**	**−21.92**	**Met**	**165**	**−27.68**	**Met**	**165**	**−18.34**	**Gln**	**189**	**−26.6855**
Met	**165**	**−19.9**	**Glu**	**166**	**−17.37**	**Gln**	**189**	**−20.89**	**His**	**41**	**−15.55**	**Met**	**165**	**−21.0185**
Asn	**142**	**−16.47**	**Asn**	**142**	**−17.08**	His	164	−14.33	Ser	144	−13.43	**Asn**	**142**	**−14.016**
Cys	145	−14.9	**His**	**41**	**−14.81**	Arg	188	−13.65	**Glu**	**166**	**−11.42**	**His**	**41**	**−13.3386**
His	**41**	**−12.35**	Arg	188	−14.45	Asp	187	−13.42	Cys	145	−10.96	Thr	190	−12.4393
Ser	144	−12.24	Thr	26	−11.25	Gln	192	−10.91	Met	49	−10.96	Pro	168	−11.4904
Gln	192	−11.93	Asp	187	−10.21	**Asn**	**142**	**−10.91**	**Asn**	**142**	**−10.76**	His	164	−11.258
Arg	188	−11.37	Gly	143	−9.154	Leu	167	−10.31	Gln	192	−10.59	Gly	143	−10.6192
Thr	190	−9.416	Cys	145	−9.015	**His**	**41**	**−9.586**	Gly	143	−9.827	Leu	141	−9.58516

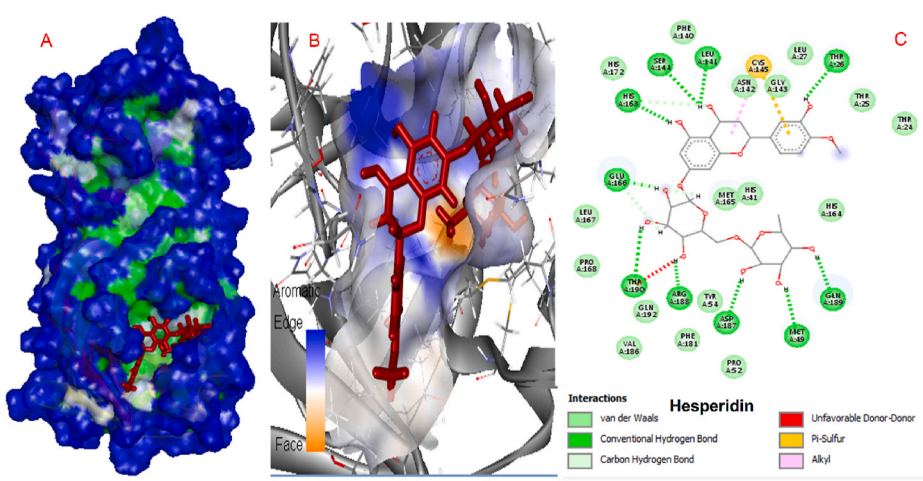

Fig. 2. Interactions of hesperidin and COVID-19 virus M^{pro}.

$$\mu = -\chi = 1/2\ (E_{LUMO} + E_{HOMO}) \quad \text{(Eq.4)}$$

$$\chi = -1/2\ (E_{LUMO} + E_{HOMO}) \quad \text{(Eq.5)}$$

The global electrophilicity (ω) chemical potential (μ), global hardness (η), global softness (S), electronegativity (χ) were calculated from

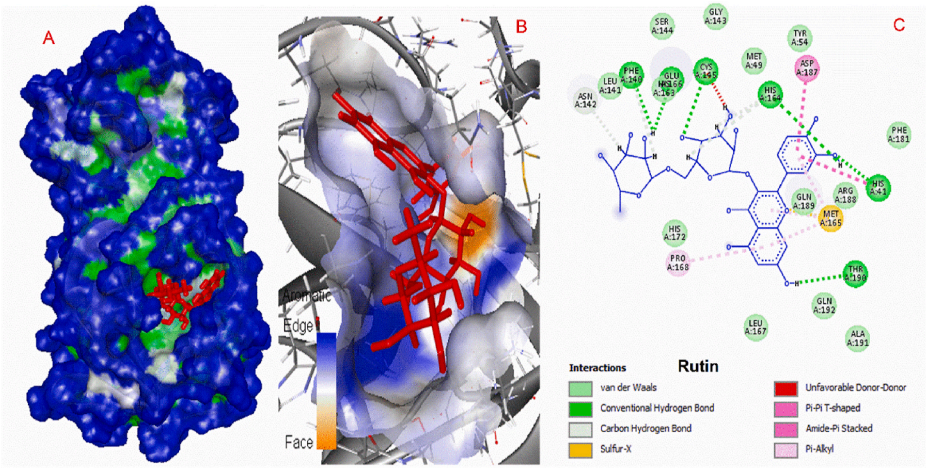

Fig. 3. Interactions of rutin and COVID-19 virus M^{pro}.

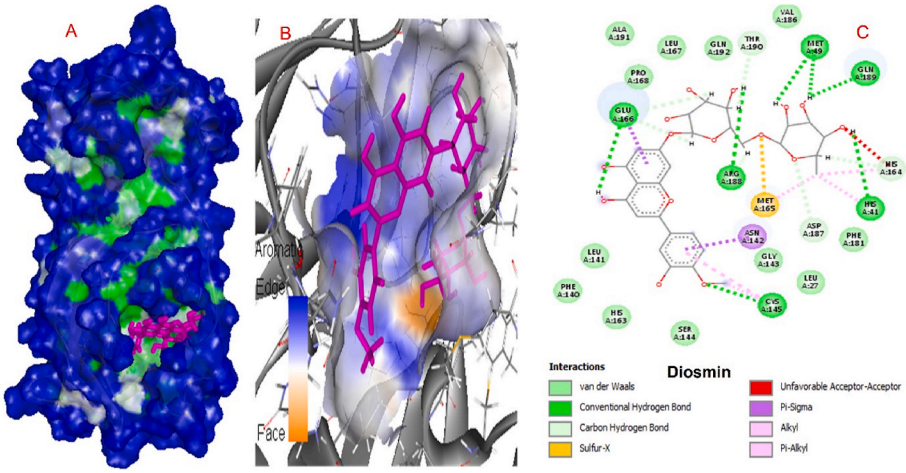

Fig. 4. Interactions of apiin and COVID-19 virus M^{pro}.

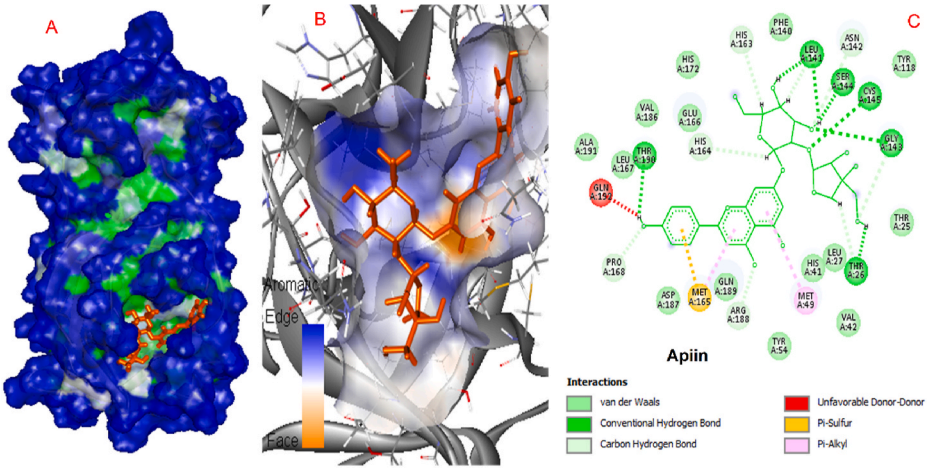

Fig. 5. Interactions of diosmin and COVID-19 virus M^{pro}.

the simulation results are presented in Table 3. The frontier orbital representations are shown in Fig. 6 for hesperidin, rutin, diosmin, apiin, and positive control nelfinavir. According to docking results, the following fitting rank among the polyphenols is determined: hesperidin > rutin > diosmin > apiin. The comparison of HOMO and LUMO energy values of polyphenols with nelfinavir, showed that the energy level of nelfinavir is lower than the polyphenols significantly for each of the frontier orbitals. Whereas, the bandgap value of nelfinavir is nearly equal to the polyphenolic compounds. Best-docked polyphenolic compound's eV values are approximately equal to each other and are in the

Table 3
Physical characteristics of computed for polyphenols (eV).

	NELFINAVIR	HESPERIDIN	RUTIN	DIOSMIN	APIIN
Total DFT-D energy (Ha)	**−2107.65**	−2213.32	−2248.04	−2212.14	−2058.34
Df binding energy (eV)	**−390.767**	−364.522	−350.602	−359.267	−325.608
E_{HOMO} (eV)	**−4.542**	−5.020	−5.361	−5.470	−5.398
E_{LUMO} (eV)	**−1.600**	−2.519	−2.196	−2.600	−2.429
Band gap ($E_{HOMO\ -\ LUMO}$) (eV)	**−2.942**	−2.501	−3.165	−2.870	−2.969
$\Delta E(E_{LUMO\text{-}HOMO})$ (eV)	**2.942**	2.501	3.165	2.870	2.969
Electronegativity (χ) (eV)	**3.071**	3.770	3.779	4.035	3.914
Chemical potential (μ) (eV)	**−3.071**	−3.770	−3.779	−4.035	−3.914
Global hardness (η) (eV)	**1.471**	1.251	1.583	1.435	1.485
Global softness (S) (eV-1)	**0.736**	0.625	0.791	0.718	0.742
Global electrophilicity index (ω) (eV)	**4.716**	7.105	7.139	8.141	7.658

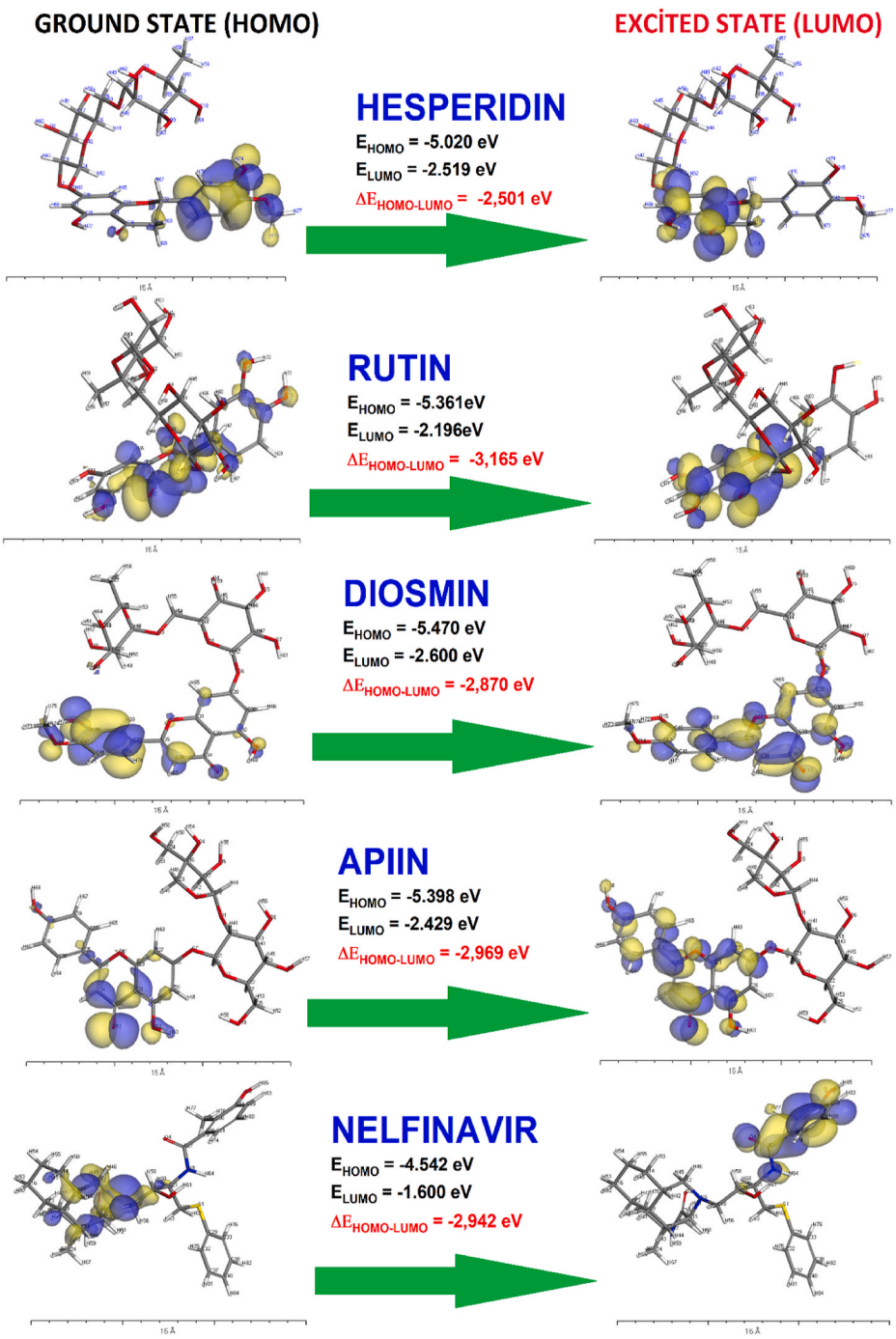

Fig. 6. 3D plots frontier orbital energies using DFT method for hesperidin, rutin, diosmin, apiin, and nelfinavir compounds.

range of −2.196 to −2.600 for LUMO and −5.020 to −5.470 for HOMO. While the eV values are 1.600 for LUMO and 4.542 for HOMO for nelfinavir.

HOMO propagation on the molecule is attributed to its ability for nucleophilic attack. LUMO is another parallel consideration can be done for the reactive ability [59]. The difference between energy values of LUMO and HOMO in interaction reveals the stimulation of the residues of the protein, which facilitates electron transitions between protein and ligand. This difference governs the magnitude of reactivity (reaction kinetic) and the stability of the molecule [60,61]. Under the light of the phenomenons, ω, μ, and χ values are significantly higher for the polyphenol compounds depending on the HOMO and LUMO energy values than nelfinavir. These values determine the global reactivity of all molecules against the target protein as seen from Table 3. The higher global electrophilicity and softness values in ligand-protein interactions can be attributed good reactivities of ligands that are expected particularly in biological system-based studies.

The propagation of HOMO and LUMO through the compounds is provided in Fig. 6. According to the figure, nucleophilic and electrophilic reactivity sides of molecules are commonly on the aromatic or phenolic sites of the compounds. As it can be seen that the HOMO-&LUMO-based reactivity of compounds against protein is compatible with the docking results especially in the conventional hydrogen bond, π- π, amide-π and π-alkyl interaction formations.

3.2.2. Local chemical reactivities by Fukui function

The Fukui function describes the electron density in the frontier orbitals depending on electrophilic, nucleophilic, and radicalic propagation. It is a useful tool to discuss the reactivity of the compounds in researches [43,44]. In the current study, the Fukui indices-based spaces were given inside the electrostatic potential map together in Fig. 7. The effective electrophilic, nucleophilic, and radicalic Fukui indices; f^-, f^+, *and* f^0 are tabulated in Table 4 identifying local reactivities of compounds. All Fukui indices containing local electrophilicity (W^-, W^+, *and* W^0) and local softness (S^-, S^+, *and* S^0) for each atom of the best effective compounds against Covid 19 are given in the supplementary documents in the range of Tables 1S–5S Also, Muliiken's atomic charges for each of the compounds are tabulated in Table 6S and the atomic charge propagation is shown Figs. 6S–10S. 2D molecular structures for easy comparison of the most effective compounds are given in supplementary files in Figs. 6S–10S. Along with the simulation results from Table 4, it can be seen that the atom number of electrophilic, nucleophilic, and radicalic character and their propagation over the hesperidin molecule are widely distributed as compared with the other molecules. Also, these characteristic atoms of the molecules are commonly located on the aromatic and phenolic regions of the molecules and they are dominant to form strong interactions against target regions of the protein. Whereas, aliphatic regions of molecules are mostly recessive and they are associated with the formation of weak interactions. So, the interaction possibility of hesperidin molecules with SARS-CoV-2 main protease is

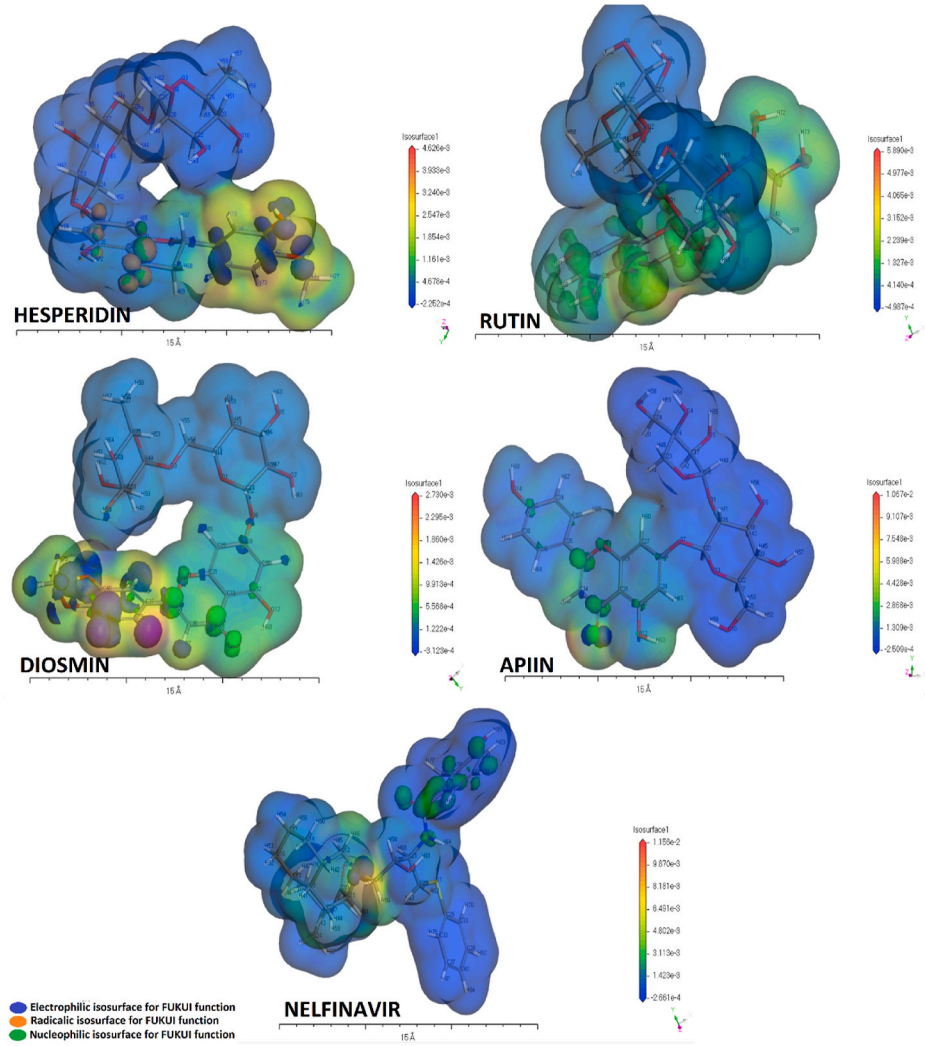

Fig. 7. Electrophilic surface-based electrostatic potential map containing the Fukui surfaces.

Table 4
Fukui (f^-, f^+, f^0) indices for electrophilic, nucleophilic and radical attack of best effective compounds against Covid 19.

THE EFFECTIVE FUKUI INDICES OF HESPERIDIN

f^-		f^+		f^+	
O14	0.126	O11	0.042	O13	0.089
O15	0.127	O12	0.06	O14	0.065
C38	0.043	O13	0.164	O15	0.066
C39	0.078	C28	0.057	C36	0.073
C40	0.059	C30	0.053	C39	0.042
C41	0.051	C35	0.057		
C42	0.059	C36	0.141		
H70	0.052	H65	0.041		
H71	0.064	H66	0.044		
H73	0.055	H68	0.053		
H75	0.047	H69	0.061		
H76	0.047				

THE EFFECTIVE FUKUI INDICES OF DIOSMIN

f^-		f^+		f^+	
O14	0.042	O11	0.047	O13	0.078
O15	0.136	O12	0.040	O15	0.077
C36	0.043	O13	0.123	C34	0.048
C38	0.051	C34	0.087	C35	0.048
C39	0.078	C35	0.077	C36	0.042
C41	0.041	C36	0.041	C38	0.042
C42	0.059	H67	0.051	C39	0.054
H69	0.048			C42	0.045
H70	0.056			H67	0.040
H71	0.047			H70	0.042

THE EFFECTIVE FUKUI INDICES OF RUTIN

f^-		f^+		f^+	
O6	0.056	O11	0.065	O6	0.039
O12	0.177	O12	0.160	O11	0.065
O15	0.043	O14	0.043	O12	0.160
O16	0.047	C30	0.072	C30	0.072
		C31	0.105	C31	0.105
		C35	0.057		
		H65	0.042		

THE EFFECTIVE FUKUI INDICES OF APIIN

f^-		f^+		f^+	
O13	0.299	O12	0.041	O11	0.048
C34	0.053	O13	0.286	O13	0.133
H62	0.058	C32	0.063	C30	0.042
		C33	0.042	C32	0.078
		C34	0.054	C33	0.074
				C34	0.043
				H62	0.053

THE EFFECTIVE FUKUI INDICES OF NELFINAVIR

f^-		f^+		f^+	
N6	0.154	O4	0.130	O4	0.071
H57	0.118	C27	0.082	N6	0.075
H56	0.068	C30	0.058	C27	0.042
H51	0.068	C39	0.099	C39	0.051
H46	0.071	H74	0.051	H57	0.063
H45	0.075	H80	0.050		
		H83	0.054		

higher than the other effective molecules.

3.2.3. Electron density analysis by Muliken's population analysis

Electron distribution over atoms inside molecules, can not be ignored because of its significant effects on the bond angles and lengths [58]. Figs. 1S–5S describes the atomic charges depending on Muliken's algorithm. The evaluation of the relationship between the molecular structures and atomic charges shows that electron density in all molecules is higher in the aromatic side of the molecules especially on (C═O, C═C, C–*O*–H) bond species. The higher charges of the H atoms can be attributed to (C = = C, H–*O*–C = = C) structures. Oxygen atoms and double-bonded oxygen atoms neighboring carbon atoms in all molecules commonly have negative charges. While the other carbon atoms have strong or slight positive charges depending on the electronegativity of the neighboring atom. Electrophilic surface-based electrostatic potential maps in Fig. 7 is coherent with electrostatic assessment of each atom in molecules. This evaluation also can be verified for nucleophilic and radicalic attacks.

3.3. Molecular dynamic studies

To further analyze the binding behavior of the natural polyphenols, molecular dynamics was utilized with the aid of NAMD software. The SARS-CoV-2 M^{pro} (PDB ID: 6Y84) with the best resolution structure was subjected to 100 ns MDS. Fig. 8A, B, and 8C summarize the simulated dynamics of the protein during the 100 ns time domain. Root Mean Square Deviation (RMSD) in Å (blue), Radius of Gyration (RoG) in Å (red), the total number of H-bonds (orange), and Surface Accessible Surface Area (SASA) in $Å^2$ (gray) are represented in Fig. 8A versus time of the simulation in nanoseconds (ns). The histogram of each parameter is depicted in Fig. 8B with the same color code. As shown from RMSD versus time and the RMSD histogram, the system is equilibrated from the first ten ns of the simulation, reaching a value of 2.2 ± 0.8 Å. Both RoG and SASA are stable during the simulation period with values 22.5 ± 0.4 Å and 15600 ± 600 $Å^2$, respectively. The total number of the H-bonds is also stable ranging from 418 to 522 during the 100 ns simulation. These values reflect the stability of the protein system during the simulation.

On the other hand, the per-residue Root Mean Square Fluctuations (RMSF) in Å are depicted in Fig. 8C. The structure of the SARS-CoV-2 M^{pro} is shown in the colored representation in Fig. 8C. As expected, the N and C terminals of the protein are highly flexible, where RMSF values are reaching 4.5 and 8.5 Å, respectively. The entire protein (green cartoon) has RMSF values ranging between 0.5 and 2 Å except for the marked two regions (residues 46–53 (blue helix) and residues 189–194 (yellow coil)). These two regions have RMSF values reaching 4.2 Å and 2.4 Å, respectively. These highly movable regions are located apart from the two active site residues (H41 and C145), represented by the red stick in Fig. 8C. In order to check the effect of protein dyanmics on binding, AutoDock Vina was utilized to dock the best four compounds from Fig. 1 into H41 and C145 of SARS-CoV-2 M^{pro}.

Fig. 8A shows the binding energies of the docking of Nelfinavir, diosmin, rutin, hesperidin, and apiin into the active site of SARS-CoV-2 M^{pro}. Here 12 different conformations of the protein are selected after clustering analysis using Chimera software. The 12 representative conformations are taken at 8.4, 10.8, 14.2, 22.7, 40.1, 44.7, 54.7, 65.0, 68.3, 75.7, 79.2, and 90.6 ns. As shown in Fig. 8C, the RMSF is stable near the active site pocket suggesting no major effect on the ligand binding. This is reflected in the average binding energies calculated from the different conformations of SARS-CoV-2 M^{pro} depicted in Fig. 8A, with the standard deviation values as the error bars. At least four compounds show better average binding affinities to SARS-CoV-2 M^{pro} compared to the positive control compound, Nelfinavir (−7.4 ± 0.6 kcal/mol). These four compounds are diosmin (−8.7 ± 0.5 kcal/mol), rutin (−8.6 ± 0.6 kcal/mol), hesperidin (−8.5 ± 0.4 kcal/mol) and apiin (−8.2 ± 0.4 kcal/mol).

The most common interactions established between the polyphenols and the SARS-CoV-2 M^{pro} are the H-bonding and hydrophobic interaction. Fig. 8B shows the interactions formed between the polyphenols (Diosmin, Rutin, Hesperidin, and Apiin) and SARS-CoV-2 M^{pro} active site residues H41 and C145 after docking. Diosmin forms seven H-bonds

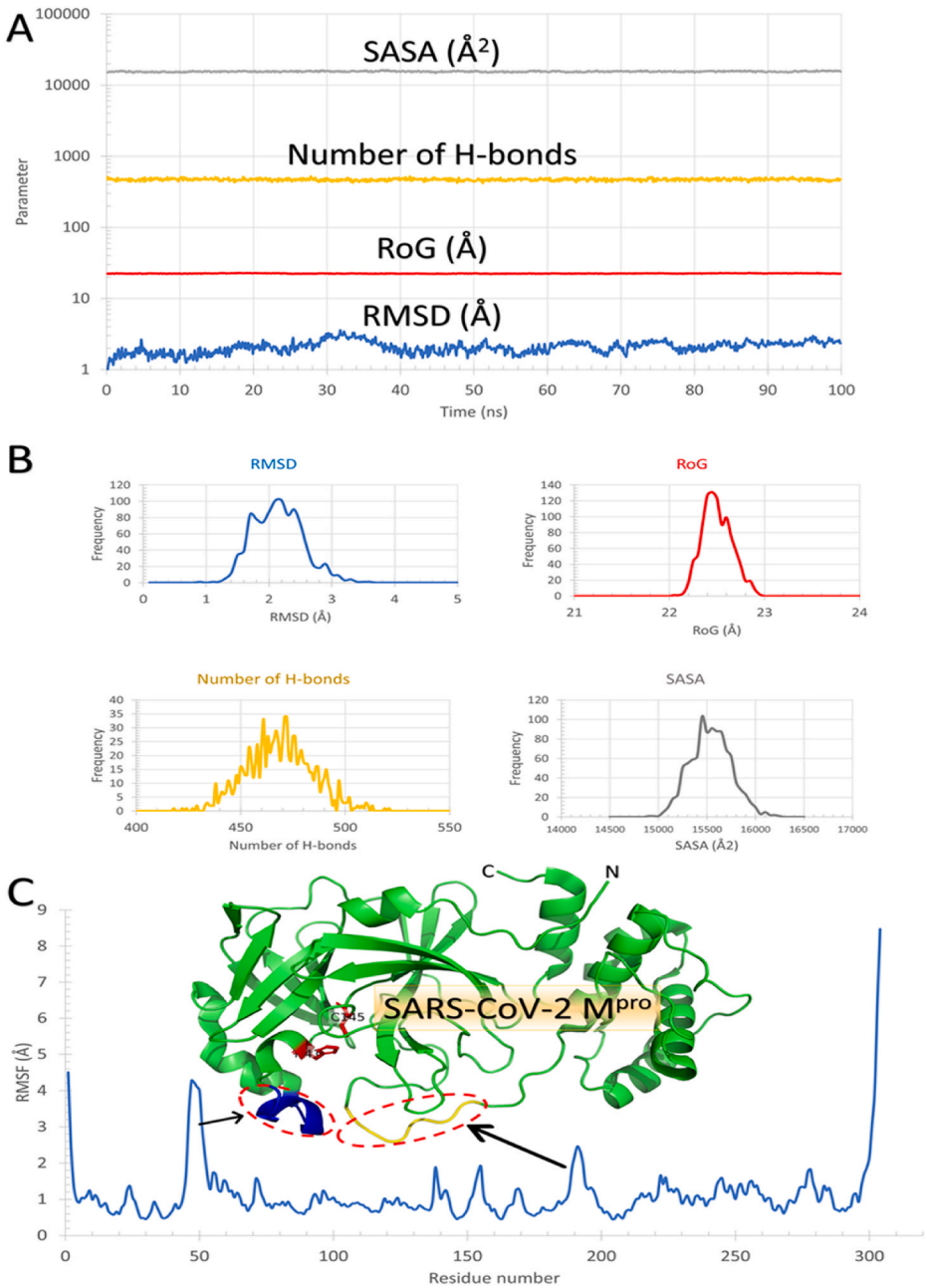

Fig. 8. Molecular Dynamics Simulation of SARS-CoV-2 M^{pro}. (A) RMSD (in Å) in blue, RoG (Å) in red, Number of H-bonds in yellow, and SASA (in $Å^2$) in gray versus time in ns. (B) Histogram of the four parameters mentioned in A with the same color code. (C) The per-residue RMSF of SARS-CoV-2 M^{pro} with the protein structure represented in the green cartoon. The most movable parts are marked in the RMSF chart and the protein structure (the encircled blue helix and yellow coil).

(L141, S144, E166, R188, Q189, T190, and Q192) and two hydrophobic contacts (E166 and P168), while both Rutin and Apiin, form eight H-bonds (T26, N142, G143, S144(2), C145, E166 and Q189 for Rutin, and T24, T26, N119, N142, G143, S144(2), and C145 for Apiin). Rutin forms three hydrophobic contacts (M165, E166, and Q189), while Apiin doesn't form any hydrophobic interactions with SARS-CoV-2 M^{pro}. Hesperidin creates fewer hydrophobic contacts (one with T25), while it establishes six H-bonds (N142, G143, S144(2), Q189, and T190) with SARS-CoV-2 M^{pro}.

As shown in Fig. 8B, the most dominant interactions are the H-bonding (blue line) in all the studied polyphenols. The most conserved H-bonds that are established in all the four polyphenols are through S144, while Rutin, Hesperidin, and Apiin form H-bonds to N142 and G143. E166 and Q189 are engaged in both H-bonds (blue lines) and hydrophobic interactions (dashed-gray lines) with Diosmin and Rutin.

3.4. ADMET studies

ADMET analysis of hit compounds is provided in Table 5. The volume of distribution at steady state (VDSS) was predicted to range from 1.663 to 0.996. They can be found at high concentrations in plasma rather than tissue. If the target is not in the brain, protecting the brain from the toxic effects of drugs is pharmacologically very important. In this model, values between 0.4- (−1) for logBB were defined as the molecule medium-level could cross the BBB, and lower than −1 poorly distributed to the brain. Nelfinavir (−0.522) indicates a low BBB permeability and these compounds (−1.715 - (−1.899) also display a poor BBB permeability. Similar results were obtained for CNS permeability studies. These results have demonstrated that the most active compounds against SARS-CoV-2 main protease had less toxicity than nelfinavir for the brain. In the evaluation of the maximum tolerated dose

Table 5
Important ADMET properties for some flavonoids with high binding affinity.

Property	Model Name	Predicted Value				
		Hesperidin	Rutin	Diosmin	Apiin	Nelfinavir
Absorption	Water solubility (log mol/L)	−3.014	−2.892	−2.929	−2.851	−3.894
	Caco2 permeability (log Papp in 10^{-6} cm/s)	0.505	−0.949	0.305	−0.966	0.693
	Intestinal absorption (human) (% Absorbed)	31.481	23.446	29.319	17.411	70.888
	Skin Permeability(log Kp)	−2.735	−2.735	−2.735	−2.735	−2.737
	P-glycoprotein substrate	Yes	Yes	Yes	Yes	Yes
	P-glycoprotein I inhibitor	No	No	No	No	Yes
	P-glycoprotein II inhibitor	No	No	No	No	Yes
Distribution	VDss (human) (log L/kg)	0.996	1.663	1.428	1.004	0.563
	Fraction unbound (human) (Fu)	0.101	0.187	0.105	0.171	0.094
	BBB permeability (log BB)	−1.715	−1.899	−1.795	−1.793	−0.522
	CNS permeability (log PS)	−4.807	−5.178	−4.836	−4.972	−2.245
Metabolism	CYP2D6 substrate	No	No	No	No	No
	CYP3A4 substrate	No	No	No	No	Yes
	CYP1A2 inhibitior	No	No	No	No	No
	CYP2C19 inhibitior	No	No	No	No	Yes
	CYP2C9 inhibitior	No	No	No	No	No
	CYP2D6 inhibitior	No	No	No	No	Yes
	CYP3A4 inhibitior	No	No	No	No	Yes
Excretion	Total Clearance(log ml/min/kg)	0.211	−0.369	−0.113	−0.054	0.399
	Renal OCT2 substrate	No	No	No	No	No
Toxicity	Max. tolerated dose (human) (log mg/kg/day)	0.525	0.452	0.565	0.446	−0.576
	hERG I inhibitor	No	No	No	No	No
	hERG II inhibitor	Yes	Yes	Yes	Yes	Yes
	Oral Rat Acute Toxicity (LD50) (mol/kg)	2.506	2.491	2.512	2.49	2.54
	Oral Rat Chronic Toxicity (LOAEL) (log mg/kg_bw/day)	3.167	3.673	3.343	4.574	3.911
	Hepatotoxicity	No	No	No	No	Yes
	Skin Sensitization	No	No	No	No	No

suggested for the human phase I study, 0.477 logs (mol/kg/day) equal or less concentration is considered low, and above it is considered high. While Rutin and Apiin have suitable values for the human phase I study suggested that, Hesperidin and Diosmin have values slightly above the recommended toxicity value. Also, their maximum tolerated dose (human) is lower Nelfinavir than. Four compounds were predicted as no potent inhibitors for CYP1A2, CYP2C19, CYP2C9, CYP2D6, CYP3A4 enzymes. Therefore, these flavonoids were predicted as nontoxic for the liver. But, Nelfinavir was found as a potential inhibitor for CYP2C19, CYP2D6, CYP3A4 enzymes, and predicted to have hepatotoxicity. In terms of other toxicity values such as hERG I inhibitor, oral rat acute toxicity (LD_{50}), oral rat chronic toxicity (LOAEL), skin sensitization, these compounds falls within acceptable range.

The antiviral effects of flavonoids have been the subject matter of several reports [62–64]. It has been previously reported that flavonoids exert their antiviral effects via blockage of cellular receptors, inhibiting viral antigenic determinants, loss of enzymatic functions, and/or inhibition of particle biosynthesis, which is consistent with our findings [65–67]. Furthermore, the antiviral activity of specific flavonoid subclass groups such as catechins, flavanones, flavonols has been reported previously against various viral strains [68,69]. Song et al. (2005) reported reduced viral infectivity by catechins [68]. Antiviral natural product-based medicines have also been used for two previous coronavirus outbreaks of SARS-CoV and MERS-CoV, which suggests that nature has tremendous potential to provide treatment for the ongoing epidemic of COVID-19 [70–72].

Previous reports also suggested the anti-influenza virus potential of Hesperidin and Apiin [73,74]. Additionally, the anti-Dengue virus (DENV) activity of Rutin [75], the anti-rotavirus potential of Diosmin, was reported [76]. Hesperidin and diosmin are flavanone glycoside, which is richly found in the citrus, including lemons, grapefruits, and sweet oranges [77,78]. Among all the flavonoids, Diosmin, Rutin, Hesperidin, and Apiin are found to possess very promising binding interactions with SARS-CoV-2 M^{pro}.

Hesperetin, a primary metabolite of hesperidin, has been shown to inhibit viral M^{pro} cleavage activity with IC_{50} of 8.3 μM [71]. Hesperidin is a readily bioavailable compound reaching a peak plasma concentration of 1.28 μmol/L in humans after intake of 1L orange juice [79]. Some studies also suggest its efficacy at the SARS-CoV-2 replication sites such as lungs. Hesperidin and Hesperetin were found to be effective in reducing the discharge of pro-inflammatory cytokines in the lungs. Hesperidin has also been reported as an effective antagonist of Th2 cytokines in the alveolar space where localized inflammatory cytokine storms arise during early phases of respiratory distress syndrome, eventually leading to organ damage [80,81]. A daily dose of 292 mg Hesperidin (500 mL of orange) resulted in significant anti-atherogenic and anti-inflammatory activities in a large-scale clinical trial [81]. As COVID-19 - patients suffer from severe inflammatory cytokine response in the later stages of infection; thus, dual antiviral/anti-inflammatory properties of this compound recommend its efficacy for the prevention and treatment of COVID-19. Interestingly, its toxicity is also low, with LD_{50} more than 4.5 g/kg [82]. Thus, hesperidin's efficacy, bioavailability, and low toxicity suggest its immense potential against COVID-19. COVID-19 patients also suffer from hypoxic pulmonary vasoconstriction and reduced lung ventilation [83]. Daflon (500 mg) is a flavonoid vasoprotective containing Diosmin (90%) and Hesperidin as active ingredients with no side effects and having $LD_{50} >$ 3 g/kg [84]. Thus, combinatorial therapies of Daflon or Hesperidin supplements with other drugs might work effectively for the treatment of COVID-19 patients.

4. Conclusion

In this study, computer-aided molecular docking was performed using 81 flavonoid-based compounds against SARS-CoV-2 M^{pro}. The most effective compounds (Hesperidin, Rutin, Diosmin, and Apiin) were studied in multiple dimensions using computer-aided simulation and computational techniques to determine their affinity, binding stability, and the closest real condition responses against SARS-CoV-2 Mpro. We found that these compounds have a better binding affinity than Nelfinavir. All the compounds bearing good binding potency are components of dietary foods, further supporting the potential of these compounds as cheaper and safer candidates to develop therapeutics against COVID-19. The study provides a scientific basis for the utilization of dietary

molecules as SARS-CoV-2 M^{pro} inhibitors, however, these in silico results need to be validated by *in vitro* protease activity assay and *in vivo* studies. Besides, the optimal dosing regimen for adults and the elderly based on reducing viral load and shortening the infectious period needs to be optimized for therapeutic implications.

Declaration of competing interest

The authors have no conflict of interest.

Acknowledgments

MDS calculations are conducted on the supercomputing facility of the Bibliotheca Alexandrina, Alexandria, Egypt. This work is done during the Junior associate award granted to the author for the period 2016–2021 from the Abdus Salam International Center for Theoretical Physics (ICTP), Trieste, Italy. The preprinted form of this paper was published in www.preprints.org with the DOI number; 10.20944/preprints202003.0333.v1 entitled "Identification of potent COVID-19 main protease (Mpro) inhibitors from natural polyphenols: an in silico strategy unveils a hope against CORONA".

Appendix A. Supplementary data

Supplementary data to this article can be found online at https://doi.org/10.1016/j.compbiomed.2022.105452.

References

[1] I. Aanouz, A. Belhassan, K. El-Khatabi, T. Lakhlifi, M. El-Ldrissi, M. Bouachrine, Moroccan Medicinal plants as inhibitors against SARS-CoV-2 main protease: computational investigations, J. Biomol. Struct. Dyn. (2020) 1–9.
[2] M.K. Gupta, S. Vemula, R. Donde, G. Gouda, L. Behera, R. Vadde, In-silico approaches to detect inhibitors of the human severe acute respiratory syndrome coronavirus envelope protein ion channel, J. Biomol. Struct. Dyn. (2020) 1–11.
[3] Y.R. Guo, Q.D. Cao, Z.S. Hong, Y.Y. Tan, S.D. Chen, H.J. Jin, K.S. Tan, D.Y. Wang, Y. Yan, The origin, transmission and clinical therapies on coronavirus disease 2019 (COVID-19) outbreak - an update on the status, Mil. Med. Res. 7 (2020) 11.
[4] R.J. Khan, R.K. Jha, G.M. Amera, M. Jain, E. Singh, A. Pathak, R.P. Singh, J. Muthukumaran, A.K. Singh, Targeting SARS-CoV-2: a systematic drug repurposing approach to identify promising inhibitors against 3C-like proteinase and 2'-O-ribose methyltransferase, J. Biomol. Struct. Dyn. (2020) 1–14.
[5] C.J. Alméciga-Díaz, L.N. Pimentel-Vera, A. Caro, A. Mosquera, C.A.C. Moreno, J.P. M. Rojas, D.C. DíazTribaldos, Virtual Screening of Potential Inhibitors for SARS-CoV-2 Main Protease, 2020.
[6] N. Yamamoto, S. Matsuyama, T. Hoshino, N. Yamamoto, Nelfinavir Inhibits Replication of Severe Acute Respiratory Syndrome Coronavirus 2 in Vitro, 2020.
[7] S. Boopathi, A.B. Poma, P. Kolandaivel, Novel 2019 coronavirus structure, mechanism of action, antiviral drug promises and rule out against its treatment, J. Biomol. Struct. Dyn. (2020) 1–10.
[8] S.A. Khan, K. Zia, S. Ashraf, R. Uddin, Z. Ul-Haq, Identification of chymotrypsin-like protease inhibitors of SARS-CoV-2 via integrated computational approach, J. Biomol. Struct. Dyn. (2020) 1–10.
[9] A. Hasan, B.A. Paray, A. Hussain, F.A. Qadir, F. Attar, F.M. Aziz, M. Sharifi, H. Derakhshankhah, B. Rasti, M. Mehrabi, K. Shahpasand, A.A. Saboury, M. Falahati, A review on the cleavage priming of the spike protein on coronavirus by angiotensin-converting enzyme-2 and furin, J. Biomol. Struct. Dyn. (2020) 1–9.
[10] R. Lu, X. Zhao, J. Li, P. Niu, B. Yang, H. Wu, W. Wang, H. Song, B. Huang, N. Zhu, Y. Bi, X. Ma, F. Zhan, L. Wang, T. Hu, H. Zhou, Z. Hu, W. Zhou, L. Zhao, J. Chen, Y. Meng, J. Wang, Y. Lin, J. Yuan, Z. Xie, J. Ma, W.J. Liu, D. Wang, W. Xu, E. C. Holmes, G.F. Gao, G. Wu, W. Chen, W. Shi, W. Tan, Genomic characterisation and epidemiology of 2019 novel coronavirus: implications for virus origins and receptor binding, Lancet 395 (2020) 565–574.
[11] R. Luthy, J.U. Bowie, D. Eisenberg, Assessment of protein models with three-dimensional profiles, Nature 356 (1992) 83–85.
[12] N. Muralidharan, R. Sakthivel, D. Velmurugan, M.M. Gromiha, Computational studies of drug repurposing and synergism of lopinavir, oseltamivir and ritonavir binding with SARS-CoV-2 protease against COVID-19, J. Biomol. Struct. Dyn. (2020) 1–6.
[13] A.D. Elmezayen, A. Al-Obaidi, A.T. Sahin, K. Yelekci, Drug repurposing for coronavirus (COVID-19): in silico screening of known drugs against coronavirus 3CL hydrolase and protease enzymes, J. Biomol. Struct. Dyn. (2020) 1–13.
[14] Z. Jin, X. Du, Y. Xu, Y. Deng, M. Liu, Y. Zhao, B. Zhang, et al., Structure-based Drug Design, Virtual Screening and High-Throughput Screening Rapidly Identify Antiviral Leads Targeting COVID-19, 2020.
[15] G. Grosso, Effects of polyphenol-rich foods on human health, Nutrients 10 (2018).
[16] N.E. Thomford, D.A. Senthebane, A. Rowe, D. Munro, P. Seele, A. Maroyi, K. Dzobo, Natural products for drug discovery in the 21st century: innovations for novel drug discovery, Int. J. Mol. Sci. 19 (2018).
[17] B. Shen, A new golden age of natural products drug discovery, Cell 163 (2015) 1297–1300.
[18] A.A. Elfiky, E.B. Azzam, Novel guanosine derivatives against MERS CoV polymerase: an in silico perspective, J. Biomol. Struct. Dyn. (2020) 1–9.
[19] M.S. Murgueitio, M. Bermudez, J. Mortier, G. Wolber, In silico virtual screening approaches for anti-viral drug discovery, Drug discovery today, Technologies 9 (2012) e219–225.
[20] A. Leach, Molecular Modelling: Principles and Applications, second ed., Prentice Hall, 2001.
[21] A.A. Elfiky, W.M. Elshemey, Molecular dynamics simulation revealed binding of nucleotide inhibitors to ZIKV polymerase over 444 nanoseconds, J. Med. Virol. 90 (2018) 13–18.
[22] A.A. Elfiky, Natural products may interfere with SARS-CoV-2 attachment to the host cell, J. Biomol. Struct. Dyn. (2020) 1–10.
[23] A.A. Elfiky, SARS-CoV-2 RNA dependent RNA polymerase (RdRp) targeting: an in silico perspective, J. Biomol. Struct. Dyn. (2020) 1–9.
[24] A.A. Elfiky, E.B. Azzam, Novel guanosine derivatives against MERS CoV polymerase: an in silico perspective, J. Biomol. Struct. Dyn. (2020) 1–9.
[25] A.A. Elfiky, A.M. Ismail, W.M. Elshemey, Recognition of gluconeogenic enzymes; Icl1, Fbp1, and Mdh2 by Gid4 ligase: a molecular docking study, J. Mol. Recogn. 33 (2020), e2831.
[26] A.A. Elfiky, A. Ismail, Molecular dynamics and docking reveal the potency of novel GTP derivatives against RNA dependent RNA polymerase of genotype 4a HCV, Life Sci. 238 (2019) 116958.
[27] M. Nabati, V. Bodaghi-Namileh, In silico study of the active components (17 alpha-ethinyl estradiol and segesterone acetate) of annovera as a novel vaginal contraceptive system by docking of their binding to estrogen and progesterone receptors, Eurasian Chem. Commun. 2 (2020) 234–246.
[28] A.S.N. Formagio, C.R.F. Volobuff, C.A.L. Kassuya, C.A.L. Cardoso, M. do Carmo Vieira, Z.V. Pereira, M.C. Bagatin, G. de Freitas Gauze, Psychotria leiocarpa extract and vincosamide reduce chemically-induced inflammation in mice and inhibit the acetylcholinesterase activity, Inflammation 42 (2019) 1561–1574.
[29] L.L. Ferreira, A.D. Andricopulo, ADMET modeling approaches in drug discovery, Drug Discov. Today 24 (2019) 1157–1165.
[30] O. Trott, A.J. Olson, AutoDock Vina: Improving the speed and accuracy of docking with a new scoring function, efficient optimization, and multithreading, J. Comput. Chem. 31 (2010) 455–461.
[31] A. Molegro, MVD 7.0 Molegro Virtual Docker, DK-8000 Aarhus C, Denmark, 2019.
[32] X. Liu, B. Zhang, Z. Jin, H. Yang, Z. Rao, The Crystal Structure of COVID-19 Main Protease in Complex with an Inhibitor N3, 2020.
[33] COVID-19 main protease with unliganded active site. http://www.rcsb.org/structure/6Y84.
[34] S. Kim, P.A. Thiessen, E.E. Bolton, J. Chen, G. Fu, A. Gindulyte, L. Han, J. He, S. He, B.A. Shoemaker, PubChem substance and compound databases, Nucleic Acids Res. 44 (2015) D1202–D1213.
[35] S. Khaerunnisa, H. Kurniawan, R. Awaluddin, S. Suhartati, S. Soetjipto, Potential Inhibitor of COVID-19 Main Protease (Mpro) from Several Medicinal Plant Compounds by Molecular Docking Study, 2020.
[36] V. 1.7.6, The PyMOL Molecular Graphics System, Version 1.7.6 Schrödinger, LLC.
[37] P. Mark, L. Nilsson, Structure and dynamics of the TIP3P, SPC, and SPC/E water models at 298 K, J. Phys. Chem. 105 (2001) 9954–9960.
[38] J.C. Phillips, R. Braun, W. Wang, J. Gumbart, E. Tajkhorshid, E. Villa, C. Chipot, R. D. Skeel, L. Kalé, K. Schulten, Scalable molecular dynamics with NAMD, J. Comput. Chem. 26 (2005) 1781–1802.
[39] Ibrahim A. Noorbatcha, A.M. Khan, H.M. Salleh, Molecular dynamics studies of human ?-Glucuronidase, Am. J. Appl. Sci. 7 (2010) 823–828.
[40] W. Humphrey, A. Dalke, K. Schulten, VMD: visual molecular dynamics, J. Mol. Graph. 14 (33–38) (1996) 27–38.
[41] A.s. Inc, Modeling and Simulation Solutions for Chemicals and Materials Research, Materials Studio (Version 5.0), 2009. San Diego, USA.
[42] X. Wu, A.K. Ray, Density-functional study of water adsorption on the (formula presented) surface, Phys. Rev. B Condens. Matter 65 (2002) 1–7.
[43] B. Delley, An all-electron numerical method for solving the local density functional for polyatomic molecules, J. Chem. Phys. 92 (1990) 508–517.
[44] B. Delley, From molecules to solids with the DMol3 approach, J. Chem. Phys. 113 (2000) 7756–7764.
[45] D.E. Pires, T.L. Blundell, D.B. Ascher, pkCSM: predicting small-molecule pharmacokinetic and toxicity properties using graph-based signatures, J. Med. Chem. 58 (2015) 4066–4072.
[46] K.K. To, I.F. Hung, J.F. Chan, K.Y. Yuen, From SARS coronavirus to novel animal and human coronaviruses, J. Thorac. Dis. 5 (Suppl 2) (2013) S103–S108.
[47] S. Pant, M. Singh, V. Ravichandiran, U.S.N. Murty, H.K. Srivastava, Peptide-like and small-molecule inhibitors against Covid-19, J. Biomol. Struct. Dyn. (2020) 1–10.
[48] J.P. Martinez, F. Sasse, M. Bronstrup, J. Diez, A. Meyerhans, Antiviral drug discovery: broad-spectrum drugs from nature, Nat. Prod. Rep. 32 (2015) 29–48.
[49] L.T. Lin, W.C. Hsu, C.C. Lin, Antiviral natural products and herbal medicines, J. Tradit., Complementary Med. 4 (2014) 24–35.
[50] M.T. Khan, A. Ali, Q. Wang, M. Irfan, A. Khan, M.T. Zeb, Y.J. Zhang, S. Chinnasamy, D.Q. Wei, Marine natural compounds as potents inhibitors against the main protease of SARS-CoV-2. A molecular dynamic study, J. Biomol. Struct. Dyn. (2020) 1–14.

[51] Umesh D. Kundu, C. Selvaraj, S.K. Singh, V.K. Dubey, Identification of new anti-nCoV drug chemical compounds from Indian spices exploiting SARS-CoV-2 main protease as target, J. Biomol. Struct. Dyn. (2020) 1–9.
[52] S.K. Sinha, A. Shakya, S.K. Prasad, S. Singh, N.S. Gurav, R.S. Prasad, S.S. Gurav, An in-silico evaluation of different Saikosaponins for their potency against SARS-CoV-2 using NSP15 and fusion spike glycoprotein as targets, J. Biomol. Struct. Dyn. (2020) 1–12.
[53] M.F. Sk, R. Roy, N.A. Jonniya, S. Poddar, P. Kar, Elucidating biophysical basis of binding of inhibitors to SARS-CoV-2 main protease by using molecular dynamics simulations and free energy calculations, J. Biomol. Struct. Dyn. (2020) 1–21.
[54] I. Abdelli, F. Hassani, S. Bekkel Brikci, S. Ghalem, In silico study the inhibition of angiotensin converting enzyme 2 receptor of COVID-19 by Ammoides verticillata components harvested from Western Algeria, J. Biomol. Struct. Dyn. (2020) 1–14.
[55] S.K. Enmozhi, K. Raja, I. Sebastine, J. Joseph, Andrographolide as a potential inhibitor of SARS-CoV-2 main protease: an in silico approach, J. Biomol. Struct. Dyn. (2020) 1–7.
[56] R.H. Refaey, M.K. El-Ashrey, Y.M. Nissan, Repurposing of renin inhibitors as SARS-COV-2 main protease inhibitors: a computational study, Virology 554 (2021) 48–54.
[57] R. Shah, A. Alharbi, A.M. Hameed, F. Saad, R. Zaky, A.M. Khedr, N. El-Metwaly, Synthesis and structural elucidation for new schiff Base complexes; conductance, conformational, MOE-docking and biological studies, J. Inorg. Organomet. Polym. 30 (2020) 3595–3607.
[58] G.A.A. Al-Hazmi, K.S. Abou-Melha, N.M. El-Metwaly, I. Althagafi, R. Zaki, F. Shaaban, Green synthesis for 3-(2-Benzoylhydrazono)-N-(pyridin-2-yl) butanamide complexes: spectral, analytical, modelling, MOE docking and biological studies, J. Inorg. Organomet. Polym. 30 (2019) 1519–1536.
[59] M.A. Mumit, T.K. Pal, M.A. Alam, M.A. Islam, S. Paul, M.C. Sheikh, DFT studies on vibrational and electronic spectra, HOMO-LUMO, MEP, HOMA, NBO and molecular docking analysis of benzyl-3-N-(2,4,5-trimethoxyphenylmethylene) hydrazinecarbodithioate, J. Mol. Struct. 1220 (2020) 128715.
[60] Z. Feng, Y. Xie, F. Hao, P. Liu, H.a. Luo, Catalytic oxidation of cyclohexane by substituted metalloporphyrins: experimental and molecular simulation, RSC Adv. 5 (2015) 101593–101598.
[61] K. Li, N. Li, N. Yan, T. Wang, Y. Zhang, Q. Song, H. Li, Adsorption of small hydrocarbons on pristine, N-doped and vacancy graphene by DFT study, Appl. Surf. Sci. 515 (2020).
[62] C. Chen, H. Qiu, J. Gong, Q. Liu, H. Xiao, X.W. Chen, B.L. Sun, R.G. Yang, (-)-Epigallocatechin-3-gallate inhibits the replication cycle of hepatitis C virus, Arch. Virol. 157 (2012) 1301–1312.
[63] K. Gescher, A. Hensel, W. Hafezi, A. Derksen, J. Kuhn, Oligomeric proanthocyanidins from Rumex acetosa L. inhibit the attachment of herpes simplex virus type-1, Antivir. Res. 89 (2011) 9–18.
[64] C. Roh, S.K. Jo, (-)-Epigallocatechin gallate inhibits hepatitis C virus (HCV) viral protein NS5B, Talanta 85 (2011) 2639–2642.
[65] E.A. Bae, M.J. Han, M. Lee, D.H. Kim, In vitro inhibitory effect of some flavonoids on rotavirus infectivity, Biological & pharmaceutical bulletin 23 (2000) 1122–1124.
[66] L.K. Chang, T.T. Wei, Y.F. Chiu, C.P. Tung, J.Y. Chuang, S.K. Hung, C. Li, S.T. Liu, Inhibition of Epstein-Barr virus lytic cycle by (-)-epigallocatechin gallate, Biochem. Biophys. Res. Commun. 301 (2003) 1062–1068.
[67] F. Calzada, R. Cedillo-Rivera, R. Bye, R. Mata, Geranins C and D, additional new antiprotozoal A-type proanthocyanidins from Geranium niveum, Planta Med. 67 (2001) 677–680.
[68] J.M. Song, K.H. Lee, B.L. Seong, Antiviral effect of catechins in green tea on influenza virus, Antivir. Res. 68 (2005) 66–74.
[69] L.A. Savi, T. Caon, A.P. de Oliveira, A.M. Sobottka, W. Werner, F.H. Reginatto, E. P. Schenkel, C.R. Barardi, C.M. Simoes, Evaluation of antirotavirus activity of flavonoids, Fitoterapia 81 (2010) 1142–1146.
[70] S.Y. Li, C. Chen, H.Q. Zhang, H.Y. Guo, H. Wang, L. Wang, X. Zhang, S.N. Hua, J. Yu, P.G. Xiao, R.S. Li, X. Tan, Identification of natural compounds with antiviral activities against SARS-associated coronavirus, Antivir. Res. 67 (2005) 18–23.
[71] C.W. Lin, F.J. Tsai, C.H. Tsai, C.C. Lai, L. Wan, T.Y. Ho, C.C. Hsieh, P.D. Chao, Anti-SARS coronavirus 3C-like protease effects of Isatis indigotica root and plant-derived phenolic compounds, Antivir. Res. 68 (2005) 36–42.
[72] K.M. Lau, K.M. Lee, C.M. Koon, C.S. Cheung, C.P. Lau, H.M. Ho, M.Y. Lee, S.W. Au, C.H. Cheng, C.B. Lau, S.K. Tsui, D.C. Wan, M.M. Waye, K.B. Wong, C.K. Wong, C. W. Lam, P.C. Leung, K.P. Fung, Immunomodulatory and anti-SARS activities of Houttuynia cordata, J. Ethnopharmacol. 118 (2008) 79–85.
[73] W. Dong, X. Wei, F. Zhang, J. Hao, F. Huang, C. Zhang, W. Liang, A dual character of flavonoids in influenza A virus replication and spread through modulating cell-autonomous immunity by MAPK signaling pathways, Sci. Rep. 4 (2014) 7237.
[74] A.L. Liu, B. Liu, H.L. Qin, S.M. Lee, Y.T. Wang, G.H. Du, Anti-influenza virus activities of flavonoids from the medicinal plant Elsholtzia rugulosa, Planta Med. 74 (2008) 847–851.
[75] k. Zandi, B.T. Teoh, S.S. Sam, W.P. F, M.R. Mustafa, S.A. Bakar, In vitro antiviral activity of Fisetin, Rutin and Naringenin against Dengue virus type-2, J. Med. Plants Res. 5 (2011) 5534–5539.
[76] S.M. Lipson, Flavonoid-associated direct loss of rotavirus antigen/antigen activity in cell-free suspension, Journal of Medicinally Active Plants 2 (2013).
[77] C.C. Hsu, M.H. Lin, J.T. Cheng, M.C. Wu, Diosmin, a citrus nutrient, activates imidazoline receptors to alleviate blood glucose and lipids in type 1-like diabetic rats, Nutrients 9 (2017).
[78] M. Hajialyani, M. Hosein Farzaei, J. Echeverria, S.M. Nabavi, E. Uriarte, E. Sobarzo-Sanchez, Hesperidin as a neuroprotective agent: a review of animal and clinical evidence, Molecules (2019) 24.
[79] C. Manach, C. Morand, A. Gil-Izquierdo, C. Bouteloup-Demange, C. Remesy, Bioavailability in humans of the flavanones hesperidin and narirutin after the ingestion of two doses of orange juice, Eur. J. Clin. Nutr. 57 (2003) 235–242.
[80] J. Pugin, G. Verghese, M.C. Widmer, M.A. Matthay, The alveolar space is the site of intense inflammatory and profibrotic reactions in the early phase of acute respiratory distress syndrome, Crit. Care Med. 27 (1999).
[81] F. Meneguzzo, R. Ciriminna, F. Zabini, M. Pagliaro, Hydrodynamic Cavitation-Based Rapid Expansion of Hesperidin-Rich Products from Waste Citrus Peel as a Potential Tool against COVID-19, 2020.
[82] Y. Li, A.D. Kandhare, A.A. Mukherjee, S.L. Bodhankar, Acute and sub-chronic oral toxicity studies of hesperidin isolated from orange peel extract in Sprague Dawley rats, Regul. Toxicol. Pharmacol. : RTP (Regul. Toxicol. Pharmacol.) 105 (2019) 77–85.
[83] I. Solaimanzadeh, Acetazolamide, nifedipine and phosphodiesterase inhibitors: rationale for their utilization as adjunctive countermeasures in the treatment of coronavirus disease 2019 (COVID-19), Cureus 12 (2020), e7343.
[84] O.C. Meyer, Safety and security of Daflon 500 mg in venous insufficiency and in hemorrhoidal disease, Angiology 45 (1994) 579–584.